MULTI-FREQUENCY DIFFUSE OPTICAL TOMOGRAPHY FOR CANCER DETECTION

Chen Chen[1]*, Venkaiah C. Kavuri*[3]*, Xinlong Wang*[2]*, Ruoyu Li*[1]*, Hanli Liu*[2]*, and Junzhou Huang*[1]

[1]Department of Computer Science and Engineering, University of Texas at Arlington
[2]Department of Bioengineering, University of Texas at Arlington
[3] University of Pennsylvania

ABSTRACT

Previous work has validated that the accuracy of absorption coefficient can be improved using frequency-domain (FD) DOT measurements with multiple modulation frequencies. In this paper, we investigate the use of multi-frequency FD-DOT to improve the recovery accuracy of scattering coefficient, which is of great interest to cancer study. A new method called the clustered sparsity reconstruction (CSR) is proposed to reconstruct the absorption and scattering coefficients jointly. We conduct numerical simulations for FD-DOT image reconstruction with multi-modulation frequencies. The numerical results show that the recovery accuracy of scattering coefficient can be significantly improved using multi-frequency data and the proposed CSR method. It is interesting to demonstrate that the combination of two modulation frequencies results in the best reconstruction accuracy in terms of contrast-to-noise ratio (CNR) and root-mean-square error (RMSE), while more number of modulation frequencies does not improve the image quality much.

Index Terms— diffuse optical tomography, clustered sparsity, image reconstruction

1. INTRODUCTION

For the past two decades, diffuse optical tomography (DOT) with near-infrared (NIR) light has been a popular non-invasive, non-radiation imaging tool to provide physiology-based functional maps about the tissue under study [1]. This technique has been widely utilized to investigate functional brain imaging and cancer imaging. Light absorption of oxygenated hemoglobin (HbO2) and deoxygenated hemoglobin (Hb) has close relation to human cerebral activities, while light scattering provides rich information on cellular and organelle densities as well as inter-cellular nucleus size within the tissue [2]. Compared with other imaging modalities, such as functional magnetic resonance imaging (fMRI), magnetic resonance imaging (MRI), DOT is more portable and cost-effective.

Corresponding: Junzhou Huang. Email: jzhuang@uta.edu. This work was partially supported by NSF IIS-1423056, CMMI-1434401, CNS-1405985.

Many previous development and investigations have focused more on how to accurately reconstruct the absorption coefficient μ_a (e.g., [3, 4]), in DOT , but less on how to improve reconstruction accuracy of the scattering coefficient, μ_s'. Several recent studies have reported that light scattering of prostate cancer is significantly altered from its normal tissue [5, 6]; the scattering coefficient can be used to distinguish normal from tumor tissue. Thus, we are interested in accurately recover μ_s' in DOT.

There are three approaches to image the optical parameters, μ_a and μ_s', in DOT: the continuous wave (CW), the time domain (TD), and the frequency-domain (FD) methods. Considering the tradeoff between imaging performance and cost, we are interested in a FD approach since it is more realistic or cost-feasible to develop a FD imaging system for cancer imaging. In FD DOT, it has been shown that higher frequencies give a better separation of absorption and scattering properties and provide a better detection of small objects [7]. However, the signal-to-noise ratio decreases when increasing the modulation frequency [3]. In this study, rather than choosing a particular frequency for imaging [7], we investigate numerically the use of a multi-frequency DOT system [3] so as to examine and understand which frequency or frequencies can provide better reconstruction quality for both μ_a and μ_s' with a reduced cross talk between them.

The numerical simulation is an ideal way to achieve this goal since the ground-truth values of the optical coefficients are known. We conduct the simulations using the NIRFAST toolbox [8], with 100 MHz, 150 MHz, 200 MHz, 250 MHz frequencies and their combinations for reconstruction. A 2D transmission geometry is used in this study. The forward problem is solved by the finite element method (FEM) and the Jacobian matrix is updated iteratively. For the inverse problem, the conventional method with Tikhonov regularization often tends to oversmooth the reconstructed images [4, 9, 10, 11]. To overcome this drawback, we propose a novel method called clustered sparsity reconstruction (CSR) to simultaneously reconstruct the absorption and scattering coefficients, which is an extension of our previous work on functional brain imaging [11]. The CSR method is motivated by the prior information that the tumor is not only sparse, but also clustered in some region(s) of the tissue. According to

978-1-4799-2374-8/15/$31.00

the structured sparsity theory [12], the reconstruction can be improved by using such prior knowledge. Specifically, we present an efficient algorithm to solve the inverse problem of multi-frequency FD DOT using the accelerated proximal gradient descent framework. By the end of this paper, our extensive simulation results show that CSR in combination with multi-frequency FD DOT measurements can significantly improve the reconstruction accuracy and reduce the cross-talk between two optical parameters.

2. NUMERICAL MODELING

2.1. Forward problem

The diffusion equation in the frequency domain can be approximated by [10]

$$\nabla \cdot D(r)\nabla\Phi(r,\omega) - [\mu_a(r) + \frac{i\omega e}{c(r)}]\Phi(r,\omega) = -S(r,\omega) \quad (1)$$

where $\Phi(r,\omega)$ is the photon fluence rate at position r, $S(r,\omega)$ is the optical light source, ω is the modulation frequency, $D(r) = 1/3[\mu_a(r)+\mu_s'(r)]$ is the diffusion coefficient, $\mu_a(r)$ is the absorption coefficient, $\mu_s'(r)$ is the scattering coefficient, $c(r)$ is the speed of the light in the medium, e is the medium's index of refraction.

The Robin boundary condition can be written as:

$$\Phi(r,\omega) + l\hat{\mathbf{n}} \cdot \nabla\Phi(r,\omega) = 0 \quad (2)$$

where $\hat{\mathbf{n}}$ denotes a vector normal to the measurement surface, l is a parameter corresponds to the internal reflection of light due to the index of refraction mismatch.

The goal of the forward problem is to estimate $\Phi(r,\omega)$, while all the other parameters are known. We use the finite element method (FEM) to solve the problem. For convenience, in the rest of this paper we use the matrix notations for short. For example, $D = D(r)$, $\mu = [D^T, \mu_a^T]^T$, $\Phi = \Phi(r,\omega)$, where ^{T} denotes the transpose.

2.2. Inverse problem using Tikhonov regularization

The inverse problem in DOT is to recover the optical parameters μ_a and μ_s' based on the measured boundary data. We aim to minimize the object function:

$$F(\mu) = ||\Phi_m - \Phi(\mu)||_2^2 \quad (3)$$

where Φ_m is the measured data, and $\Phi(\mu)$ is the calculated data using the forward solver given μ. This leads to a nonlinear optimization problem. A possible way is to update μ iteratively based on the first order Taylor expansion. This problem is often severely ill-posed, due to the limited number of sources/detectors. The conventional ℓ_2 norm (Tikhonov) regularization is widely used, and the inverse problem can be written as:

$$\min_{\triangle\mu} ||\triangle\Phi - J\triangle\mu||_2^2 + \lambda||\triangle\mu||_2^2 \quad (4)$$

where J is the Jacobian matrix and $\triangle\Phi$ is the change of measurement data, λ is a positive regularization parameter and $\triangle\mu$ is the change of μ. It has a closed form solution $\triangle\mu = (J^TJ + \lambda I)^{-1}J^T\triangle\Phi$, where I denotes the identity matrix. In multi-frequency DOT, it has the following form:

$$J = \begin{bmatrix} J(\omega_1) \\ J(\omega_2) \\ J(\omega_3) \\ ... \\ J(\omega_f) \end{bmatrix}, \ \triangle\Phi = \begin{bmatrix} \triangle\Phi(\omega_1) \\ \triangle\Phi(\omega_2) \\ \triangle\Phi(\omega_3) \\ ... \\ \triangle\Phi(\omega_f) \end{bmatrix} \quad (5)$$

where $J(\omega_i)$ denotes the Jacobian matrix corresponding to the modulation frequency ω_i, and f denotes the total number of frequencies. The measurements are the combinations of each measurement vector of a single frequency. With some initial guess μ^0, we could use the forward solver to calculate $\Phi(\mu^0)$ and J^0. Then μ can be updated by $\triangle\mu$ obtained above. We iteratively update μ, J and $\Phi(\mu)$ till convergence.

3. INVERSE PROBLEM USING CLUSTERED SPARSITY REGULARIZATION

The conventional method with Tikhonov regularization tends to oversmooth the image by penalizing large coefficients, which has been observed in many existing works [4, 9, 10]. With the emerging of compressive sensing theory [13], sparsity regularization is used to improve the reconstruction quality in these works. It is assumed that the area of change of in optical parameters is relatively small compared to the entire imaging area. We further observe that a DOT image often has clustered appearance, i.e. the change of absorption or scattering often clusters in certain regions but not random distributed. In functional brain imaging, the idea of clustered sparsity regularization works well because our physical and/or behavioral actions are controlled by a certain region or clustered regions of brain activations [11]. For cancer imaging, CSR may also function well since the cancer region(s) should be small and clustered for an early stage of cancer.

With this rationale, we model the inverse problem of FD DOT as a clustered sparsity regularization problem, which is an extension to the standard sparsity regularization used in existing methods. Based on the structured sparsity theory [12], CSR leads to several advantages: 1) it can reduce the required number of measurements for successful recovery of optical properties; 2) with the same number of measurements, it will improve the recovery accuracy; 3) it will provide robustness or higher tolerance to noise. It has been proved that only $\mathcal{O}(K + C\log(N/C))$ measurements are required to recover clustered sparse signals instead of $\mathcal{O}(K + K\log(N/K))$ for standard sparse signals. Here K is the non-zero entries, N is the total number of pixels and C denotes the number of clusters with $C << K$ [12].

We assign each pixel with its 4 neighbor pixels into a group. With this group setting, the imaging problem can be

formulated as:

$$\min_{\triangle\mu_a,\triangle D}\{\frac{1}{2}||\triangle\Phi - J\triangle\mu||_2^2 + \lambda_a||\triangle\mu_a||_{2,1} + \lambda_D||\triangle D||_{2,1}\} \quad (6)$$

where $||x||_{2,1} = \sum_g ||x_g||_2$, g denotes one of the groups described above and x_g denotes the components in this group, λ_a and λ_D are two positive parameters. Note that $\triangle\mu = \begin{bmatrix}\triangle D \\ \triangle\mu_a\end{bmatrix}$ here. This modeling will make the non-zero pixels of the reconstructed image be only in the same groups, leading to the clustered structure of the non-zero pixels [14, 15].

This optimization problem is not easy to solve due to the non-smoothness and non-separability of the $\ell_{2,1}$ norm with overlapping. The first term $f(\triangle\mu) = \frac{1}{2}||\triangle\Phi - J\triangle\mu||_2^2$ is convex and smooth, and its gradient has Lipschitz constant L. Therefore, we solve this problem with the accelerated proximal gradient descent framework [16, 17]. It has been proved that such algorithm has the optimal convergence rate among first order methods [16]. We summarize the whole algorithm in Algorithm 1. There are two subproblems in the Steps 2) and 3), which are solved by the existing reweighted least squares algorithm [18].

Algorithm 1 CSR reconstruction for the inverse problem (6)

input: $\triangle\Phi$, J, λ_D, λ_a, $t^1 = 1$, $\triangle D^0$, $\triangle\mu_a^0$, $k = 0$, L

repeat

1) $\begin{bmatrix}v_1 \\ v_2\end{bmatrix} = \begin{bmatrix}\triangle D^k \\ \triangle\mu_a^k\end{bmatrix} - J^T(J\begin{bmatrix}\triangle D^k \\ \triangle\mu_a^k\end{bmatrix} - \triangle\Phi)/L$

2) $y_1^k = \arg\min_y\{\frac{L}{2}\|y - v_1\|_2^2 + \lambda_D\|y\|_{2,1}\}$

3) $y_2^k = \arg\min_y\{\frac{L}{2}\|y - v_2\|_2^2 + \lambda_a\|y\|_{2,1}\}$

4) $t^{k+1} = [1 + \sqrt{1 + 4(t^k)^2}]/2$

5) $\triangle D^{k+1} = y_1^k + \frac{t^k - 1}{t^{k+1}}(y_1^k - y_1^{k-1})$

6) $\triangle\mu_a^{k+1} = y_2^k + \frac{t^k - 1}{t^{k+1}}(y_2^k - y_2^{k-1})$

7) $k = k + 1$

until Stop criterions

4. RESULTS

The simulations are conducted using NIRFAST toolbox [8]. We use a 2D circular mesh consisting of 1785 nodes corresponding to 3418 linear triangular elements. The radius of the model was 43 mm and the background optical properties are $\mu_a = 0.1$ cm^{-1} and $\mu_s' = 10$ cm^{-1}. Three anomalies are placed in the mesh. Each of them has a radius of 7.5 mm, which is shown in Fig. 1 (a). Region A contains $\triangle\mu_a = 0.05\ cm^{-1}$ only and Region B contains $\triangle\mu_s' = 5\ cm^{-1}$ only. Region C contains both $\triangle\mu_a$ and $\triangle\mu_s'$ with the same values. There are total 16 sources and 16 detectors around the mesh. We empirically select $\lambda_D = 0.015$, $\lambda_a = 0.0005$ for CSR in this study. The conventional Tikhonov regularization in NIRFAST is used for result comparisons.

Four modulation frequencies of 100 MHz, 150 MHz, 200 MHz, 250 MHz and their combinations are used to simulate

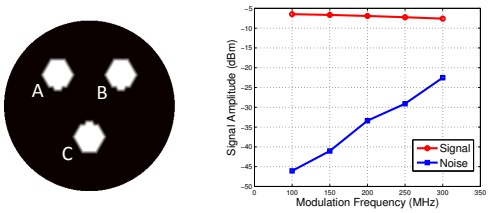

(a) (b)

Fig. 1. (a) The anomalies of the simulation. (b) The noise levels of different modulation frequencies.

acquired multi-frequency data and their respective DOT reconstructions. Therefore, there are 15 frequency combinations in total including single frequency cases. In this study, we do not use a frequency higher than 300 MHz, as higher frequency measurements are more sensitive to noise and the light can not go or penetrate deep in the tissue. We follow the previous work [3] to simulate the noises for different modulation frequencies, which are shown in Fig. 1 (b). To avoid randomness, we repeat the simulation at each frequency setting 20 times and report the average results and standard derivations (STD). Contrast-to-noise ratio (CNR) [11] and root-mean-square error (RMSE) are used as metrics for result evaluation.

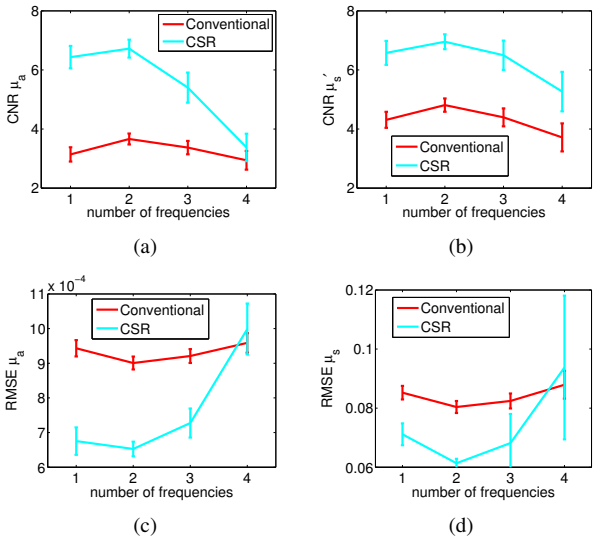

Fig. 2. The best results using different numbers of frequencies. (a) CNR values of μ_a. (b) CNR values of μ_s'. (c) RMSE values of μ_a. (d) RMSE values of μ_s'.

We select the best reconstruction results using 1 to 4 frequencies. For example, the best result by single frequency is from 200 MHz. The CNR and RMSE values of the reconstruction results are shown in Fig. 2. It shows that the combination of two modulation frequencies (100 MHz and 150 MHz) results in the highest CNR values and lowest RMSE

values. The error bars shows that the results by three or four modulation frequencies have larger STDs. This is expected due to the bigger noise contained in higher frequencies data. With proper frequencies, the proposed CSR significantly outperforms the conventional Tikhonov regularization.

The average reconstructed images are shown in Fig. 3. It is obvious that the results by CSR have much higher contrast than those by the conventional method. With respect to the signal magnitude, the conventional method has much larger cross-talk errors in the reconstructed μ_s' than CSR. Compared with the results by single frequency, it shows that using two frequencies (i.e., 100+150 MHz) could significantly improve the accuracy of μ_s' by CSR. With more number of frequencies, the accuracy of μ_s' is difficult to be further enhanced.

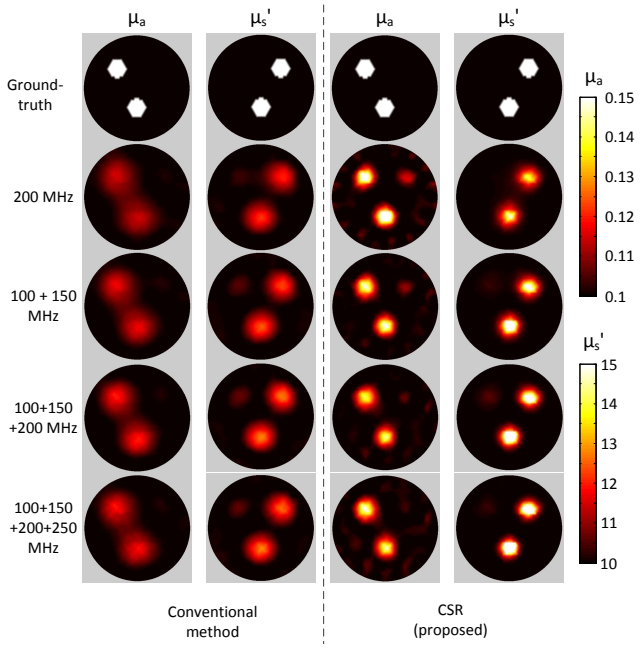

Fig. 3. The reconstructed images with different combinations of modulation frequencies (cm^{-1}). Best viewed on screen.

5. CONCLUSION

In this paper, we have proposed a new method to reconstruct the optical parameters using multi-frequency DOT measurement data. It is motivated by the sparseness and clustered appearance of the anomalies in many biomedical applications. Extensive numerical simulations show that the proposed method, namely, clustered sparsity reconstruction (CSR), consistently outperforms the conventional method with proper frequency settings. Compared with the conventional Tikhonov regularization, CSR could reduce the cross-talk artifacts of μ_s' and improve the recovery accuracy of μ_s', which makes our new algorithm potentially useful for cancer imaging.

6. REFERENCES

[1] T. Durduran, R. Choe, W.B. Baker, and A.G. Yodh, "Diffuse optics for tissue monitoring and tomography," *Rep. Prog. Phys.*, vol. 73, no. 7, pp. 076701, 2010.

[2] S. Thomsen and D. Tatman, "Physiological and pathological factors of human breast disease that can influence optical diagnosisa," *Annals of the New York Academy of Sciences*, vol. 838, no. 1, pp. 171–193, 1998.

[3] M. B. Unlu, O. Birgul, R. Shafiiha, G. Gulsen, and O. Nalcioglu, "Diffuse optical tomographic reconstruction using multifrequency data," *Journal of Biomedical Optics*, vol. 11, no. 5, pp. 054008–054008, 2006.

[4] M. Süzen, A. Giannoula, and T. Durduran, "Compressed sensing in diffuse optical tomography," *Opt. Express*, vol. 18, no. 23, pp. 23676–23690, 2010.

[5] T. C. Zhu, J. C. Finlay, and S. M. Hahn, "Determination of the distribution of light, optical properties, drug concentration, and tissue oxygenation in-vivo in human prostate during motexafin lutetium-mediated photodynamic therapy," *Journal of Photochemistry and Photobiology B: Biology*, vol. 79, no. 3, pp. 231–241, 2005.

[6] V. Sharma, E. O. Olweny, P. Kapur, J. A. Cadeddu, C. G. Roehrborn, and H. Liu, "Prostate cancer detection using combined autofluorescence and light reflectance spectroscopy: ex vivo study of human prostates," *Biomedical Opt. Express*, vol. 5, no. 5, pp. 1512–1529, 2014.

[7] H. K. Kim, U. J. Netz, J. Beuthan, and A. H. Hielscher, "Optimal source-modulation frequencies for transport-theory-based optical tomography of small-tissue volumes," *Opt. Express*, vol. 16, no. 22, pp. 18082–18101, 2008.

[8] H. Dehghani, M. E. Eames, P. K. Yalavarthy, S. C. Davis, S. Srinivasan, C. M. Carpenter, B. W. Pogue, and K. D. Paulsen, "Near infrared optical tomography using NIRFAST: Algorithm for numerical model and image reconstruction," *Communications in numerical methods in engineering*, vol. 25, no. 6, pp. 711–732, 2009.

[9] J. Prakash, C. Shaw, R. Manjappa, R. Kanhirodan, and P. K. Yalavarthy, "Sparse recovery methods hold promise for diffuse optical tomographic image reconstruction," *IEEE J. Sel. Topics Quantum Electron., to appear*, 2014.

[10] O. Lee and J. C. Ye, "Joint sparsity-driven non-iterative simultaneous reconstruction of absorption and scattering in diffuse optical tomography," *Opt. Express*, vol. 21, no. 22, pp. 26589–26604, 2013.

[11] C. Chen, F. Tian, H. Liu, and J. Huang, "Diffuse optical tomography enhanced by clustered sparsity for functional brain imaging," *IEEE Trans. Med. Imag.*, vol. 33, no. 12, pp. 2323–2331, 2014.

[12] J. Huang, T. Zhang, and D. Metaxas, "Learning with structured sparsity," *J. Mach. Learn. Res.*, vol. 12, pp. 3371–3412, 2011.

[13] E. Candes, J. Romberg, and T. Tao, "Robust uncertainty principles: Exact signal reconstruction from highly incomplete frequency information," *IEEE Trans. Inf. Theory*, vol. 52, no. 2, pp. 489–509, 2006.

[14] M. Yuan and Y. Lin, "Model selection and estimation in regression with grouped variables," *Journal of the Royal Statistical Society: Series B (Statistical Methodology)*, vol. 68, no. 1, pp. 49–67, 2006.

[15] L. Jacob, G. Obozinski, and J. Vert, "Group lasso with overlap and graph lasso," in *Proc. Int. Conf. Mach. Learn. (ICML)*, 2009.

[16] A. Beck and M. Teboulle, "A fast iterative shrinkage-thresholding algorithm for linear inverse problems," *SIAM J. Imag. Sci.*, vol. 2, no. 1, pp. 183–202, 2009.

[17] J. Huang, S. Zhang, and D. Metaxas, "Efficient mr image reconstruction for compressed mr imaging," *Medical Image Analysis*, vol. 15, no. 5, pp. 670–679, 2011.

[18] C. Chen, J. Huang, L. He, and H. Li, "Preconditioning for accelerated iteratively reweighted least squares in structured sparsity reconstruction," in *Proc. IEEE Conf. Comput. Vis. Pattern Recogn. (CVPR)*, 2014.